An Adaptive Synchronous Reference Frame Phase-Locked Loop for Power Quality Improvement in a Polluted Utility Grid

Abstract— **The proper operation of the grid-connected power electronics converters usually needs using some kind of synchronization technique in order to estimate the phase of the grid voltage. The performance of this synchronization technique is of a great importance when trying to improve the quality of the consumed or delivered electric power. The synchronous reference frame phase-locked loop (SRF-PLL) synchronization algorithm has been widely used in recent years due to its ease of operation and robust behavior. However, the estimated phase can have a considerable amount of unwanted ripple if the grid voltage disturbances (e.g. harmonic distortion and unbalance) are not properly rejected. The aim of this paper is to propose an adaptive SRF-PLL which is able to strongly reject the aforementioned disturbances even if the fundamental frequency of the grid voltage varies. This synchronization method will allow the designer to easily upgrade an existing SRF-PLL, thus improving the performance of working power converters. This is accomplished by using several adaptive Infinite Impulse Response (IIR) notch filters, implemented by means of an inherently stable Schur-lattice structure. Besides the stability properties, this structure accomplished the most important topics required to be programed into the commonly used fixed point DSPs (i.e. high mapping precision, low round-off accumulation, suppression of quantization limit cycle oscillations). The proposed adaptive SRF-PLL has been tested by programing the algorithm into the fixed-point digital signal processor TI TMS320F2812. The obtained experimental results show up that the proposed synchronization method highly rejects the undesired harmonics, even if the fundamental harmonic frequency of a highly polluted grid voltage abruptly varies.**

Index Terms— **Phase locked loop, power system harmonics, power grids, power quality, three-phase electric power, adaptive signal processing, adaptive filters, lattice filters.**

I. INTRODUCTION

The advent of renewable energy sources in conjunction with the distributed generation in a microgrid environment is rapidly changing the electric generation paradigm [1], [2]. Traditional centralized power plants will be working together with distributed generators and even with alternative energy storage systems as the electric vehicle [3], [4]. Most of the technological challenges involving this new scenario are being solved through technical solutions based on the power electronics control field.

One important issue to be solved when managing the power delivered by distributed generators, is the correct synchronization with the electric grid [5-7]. Information about the instantaneous phase of the grid voltage is needed to obtain the reference of the current delivered by the power electronics converter [8-11]. This implies that the quality of the injected power is highly related with the accuracy of this information. Despite the fact that several techniques could be used to carry out the synchronization with the grid, the state of the art suggests the use of the Synchronous Reference Frame Phase-Locked Loop (SRF-PLL) to estimate the instantaneous grid voltage phase [12-15]. The SRF-PLL needs the three-phase grid voltage to be projected from the Natural Reference Frame (NRF) into the Synchronous Reference Frame (SRF). A simple closed-loop control scheme by means of a proportional-integral (PI) regulator can be used to estimate the electric grid voltage phase [16].

Several studies have been made that allow to affirm that the SRF-PLL gives an accurate phase grid estimation if the electric grid is not polluted (i.e. the grid voltage is balanced and it does not contain harmonics different from the fundamental). However, this PLL inserts a certain amount of distortion when the point of common coupling (PCC) of the power electronics converter is polluted [16-18]. Taking into account that the estimated phase is used for synthesizing the reference of the injected current, the estimated phase imperfections deteriorate the quality of the power delivered to the utility grid. In many cases, this could not be acceptable, since the current standards and recommendations regarding distributed resources limit the maximum current distortion [19], [20].

In order to avoid the grid disturbances to affect the phase estimation, a carefully choice of the tuning parameters of the PI regulator has to be done, so that a good disturbance rejection is obtained [21]. However, this approach makes the SRF-PLL extremely slow if a good rejection of the unbalance disturbance is required. In [22], a feedforward action is used to improve the phase estimation speed, which is intended to compensate for the poor transient behavior introduced by the low-pass filter used to attenuate the utility grid disturbances. Moreover, in [23], [24] several methods are presented that allow to reject undesired ripple in the estimated phase. Nevertheless, the behavior of the proposed method is not studied when a variation in the grid frequency takes place (e.g. in a microgrid working in the islanding mode [25], [26]).

In order to take into account the grid frequency variation, [27] and [28] propose a simple structure of adaptive resonant filters. This technique allows rejecting the variable frequency harmonics that could appear in the estimated phase. Although it allows obtaining a first approach to the solution of the grid frequency variation problem, it should be noted that the stability of the adaptive method is not well studied. The stability study is mandatory since the proposed filters are implemented by means of a direct form infinite impulse response (IIR) structure, which in turn could be unstable if not correctly adjusted. Moreover, the proposed filters need a reference to track the grid frequency variation. As this reference is obtained by means of the initially polluted estimated frequency, the obtained IIR filter will start swinging until it becomes unstable. In [29], a lead compensator is introduced which claims to obtain a fast tracking of the grid voltage phase. In order to adapt the center frequency of the lead compensator, the frequency estimated by the SRF-PLL is used. However, a low-pass filter with low cut-off frequency is introduced to avoid oscillations and instability in steady-state. Therefore, the bandwidth of the SRF-PLL is highly limited by this low-pass filter, instead of by the loop-gain of the control loop. Furthermore, the stability of the lead compensator when the coefficients are real-time varied is not studied, so that the stability of the whole system could not be assured under all circumstances.

There are other methods which assure stability in the adaptive process. In [30] it is proposed a method based on a multiple synchronous reference frame to detect the positive and the negative sequence grid voltage components. In [31], a method to detect the fundamental frequency of the utility grid regardless of the presence of unbalance or harmonic distortion is shown. However, the complexity of the estimation process increase notably respect to the SRF-PLL algorithm.

The aim of this paper is to propose a phase estimator based on the well-known SRF-PLL, which has a high rejection of the disturbances introduced by the voltage unbalance and by the voltage harmonic distortion, regardless of the grid frequency variation. The system is based on the adaptive filtering of the harmonics that appear on the grid voltage projection into the SRF, when the utility grid is unbalanced and distorted. On one hand, the adaptive nature of the filtering process makes the rejection insensitive to the grid frequency variation. On the other hand, the Schur-lattice IIR structure used to implement the filter stage makes the stability of the phase estimator independent of the adaptive process. In fact, the filter is inherently stable, and does need neither any reference to be properly tuned nor added filtering stage to avoid swinging. Moreover, the proposed IIR structure makes this technique a suitable choice for fixed point DSPs, or even for cheap fixed point dsPICs, due to its low round-off noise and its ease to remove quantization limit cycles. These properties allow obtaining two major benefits [32]; the mapping of the control loop transfer functions poles and zeros are more precise, and the quantization limit cycles can be easily removed, thus avoiding swinging in the adaptive process. Furthermore, existing SRF-PLL source codes in working power converters could be easily updated in order to obtain the adaptive rejection feature.

The paper is organized as follows. In Section II, a model of the conventional SRF-PLL is shown along with the conventional PI control scheme. Furthermore, the behavior of the SRF-PLL is studied when the voltage grid is polluted. In Section III, a first approach to cancel out the harmonics in the estimated phase when the voltage grid is polluted is shown. This technique is based on IIR notch filters tuned at fixed frequencies. Section IV presents an adaptive IIR notch filter algorithm that is able to adaptively tune its center frequency, without the need of a given reference. The inherently stable operation of this filter is also probed in this section. This algorithm allows the SRF-PLL to successfully reject the undesired harmonics even if the voltage grid frequency varies. In Section V, experimental results are shown. Finally, an Appendix is added with the pseudo-code to be added to the SRF-PLL, so that it becomes adaptive.

II. The SRF-PLL

A. Modeling and Control of the SRF-PLL

The conventional SRF-PLL is based on the projection of the utility grid voltage shown by (1) from the NRF into the SRF. Fig. 1(a) shows the basic block diagram of the SRF-PLL. The PI regulator described by (2) and an integrator along with the non-linear rotation matrix shown by (3) are used in the closed loop control scheme.

In order to adjust the PI regulator, a small signal linear model of the SRF-PLL can be derived [16], thus obtaining the block diagram depicted in Fig. 1(b). In this figure, p is the grid disturbance signal, v_q is the grid voltage q axis projection into

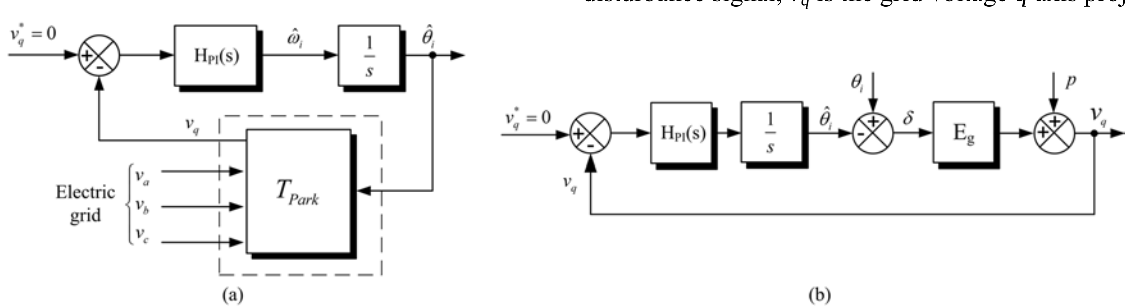

Fig. 1. (a) Basic block diagram and (b) small signal block diagram of a SRF-PLL

$$\vec{v}_g(t)=\begin{bmatrix} v_a(t) \\ v_b(t) \\ v_c(t) \end{bmatrix} = V_1 \cdot \begin{bmatrix} \cos(\theta_i) \\ \cos\left(\theta_i-\frac{2\pi}{3}\right) \\ \cos\left(\theta_i+\frac{2\pi}{3}\right) \end{bmatrix} \quad (1)$$

$$H_{PI}(s)=-K_p\cdot\left(1+\frac{K_i}{s}\right) \quad (2)$$

$$T_{park}=\sqrt{\frac{2}{3}}\begin{bmatrix} \cos(\hat{\theta}_i) & \cos\left(\hat{\theta}_i-\frac{2\pi}{3}\right) & \cos\left(\hat{\theta}_i+\frac{2\pi}{3}\right) \\ -\sin(\hat{\theta}_i) & -\sin\left(\hat{\theta}_i-\frac{2\pi}{3}\right) & -\sin\left(\hat{\theta}_i+\frac{2\pi}{3}\right) \\ \frac{1}{\sqrt{2}} & \frac{1}{\sqrt{2}} & \frac{1}{\sqrt{2}} \end{bmatrix} \quad (3)$$

the SRF, v_q^* is the reference of this projection, θ_i and $\hat{\theta}_i$ are the grid phase and the estimated grid phase respectively, and δ is the error between the actual and the estimated grid phase. This model allows to derive the open loop gain expressed by (4) and the transfer function between the estimated phase, $\hat{\theta}_i$, and the grid disturbances, p, depicted in (5). These transfer functions are used to study the stability and the effect of the grid disturbances on the estimated phase respectively. It should be considered that the rotation matrix gain, E_g, is characterized by (6), where V_1 is the amplitude of the grid voltage fundamental harmonic in the NRF.

$$T_{PLL}(s)=-E_g\cdot H_{PI}(s)\cdot\frac{1}{s} \quad (4)$$

$$G_{\theta\_p}(s)=\frac{\hat{\theta}_i}{p}=\frac{1}{E_g}\frac{T_{PLL}(s)}{1+T_{PLL}(s)} \quad (5)$$

$$E_g=\sqrt{\frac{3}{2}}V_1 \quad (6)$$

B. The SRF-PLL applied to a Polluted Grid

The electric grid is usually represented by the ideal expression shown by (1). However, the voltage at the PCC often contains harmonics other than the fundamental, as well as a certain amount of unbalance. To take these non-idealities into account (7) could be used instead.

It is worth pointing out that the most usual non-linear loads connected to the PCC, are three-phase full bridge controlled and non-controlled line frequency rectifiers. Therefore, the even and the triplen harmonics are considered to be zero [33], [34]. By applying the transformation matrix (3) to (7), and taking into account that (8) holds in the steady-state, (9) can be derived, where E_{pu}, ϕ_{pu} and δ are defined in (10), (11) and (12) respectively [16], [18], [30].

By carefully examining (9), it can be concluded that the absence of unbalance ($\beta=\gamma=0$) and harmonic distortion in the grid voltage results in the expression for the q term, $v_q=E_g\delta$. This expression can be derived from Fig. 1(b) by considering the disturbance to be zero ($p=0$). Therefore, it can be concluded that the disturbance introduced in the SRF by the unbalance and the distortion of the grid voltage can be expressed by (13) and (14) respectively.

$$\vec{v}_g=\begin{bmatrix} V_1\cos(\theta_i)-V_5\cos(5\theta_i)+V_7\cos(7\theta_i)-V_{11}\cos(11\theta_i)+\ldots \\ (1+\beta)\cdot\left(V_1\cos\left(\theta_i-\frac{2\pi}{3}\right)-V_5\cos\left(5\left(\theta_i-\frac{2\pi}{3}\right)\right)+\ldots\right) \\ (1+\gamma)\cdot\left(V_1\cos\left(\theta_i+\frac{2\pi}{3}\right)-V_5\cos\left(5\left(\theta_i+\frac{2\pi}{3}\right)\right)+\ldots\right) \end{bmatrix} \quad (7)$$

$$\hat{\theta}_i\approx\theta_i\rightarrow\theta_i+\hat{\theta}_i\approx 2\theta_i \quad (8)$$

$$v_q=E_g\delta\cdot\left(\frac{3+\gamma+\beta}{3}\right)+E_gE_{pu}\cos\left(2\theta_i-\phi_{pu}\right)+ \\ +\sqrt{\frac{3}{2}}(V_5+V_7)\cdot\cos\left(6\theta_i+\frac{\pi}{2}\right)+\sqrt{\frac{3}{2}}(V_{11}+V_{13})\cdot\cos\left(12\theta_i+\frac{\pi}{2}\right)+\ldots \quad (9)$$

$$E_{pu}=\sqrt{\left(\frac{(\gamma-\beta)}{2\sqrt{3}}\right)^2+\left(\frac{(\gamma+\beta)}{6}\right)^2} \quad (10)$$

$$\phi_{pu}=\tan^{-1}\left(\frac{\sqrt{3}}{3}\frac{(\gamma+\beta)}{(\gamma-\beta)}\right) \quad (11)$$

$$\delta=\theta_i-\hat{\theta}_i \quad (12)$$

$$P_{qu}=E_g\delta\cdot\left(\frac{3+\gamma+\beta}{3}\right)+E_gE_{pu}\cos\left(2\theta_i-\phi_{pu}\right) \quad (13)$$

$$P_{qd}=\sqrt{\frac{3}{2}}(V_5+V_7)\cdot\cos\left(6\theta_i+\frac{\pi}{2}\right)+ \\ +\sqrt{\frac{3}{2}}(V_{11}+V_{13})\cdot\cos\left(12\theta_i+\frac{\pi}{2}\right)+\ldots \quad (14)$$

An important issue that should be taken into account is that the disturbance in the q term of the SRF projection pollutes the phase estimated by the SRF-PLL. Indeed, by taking into account (12) and that $v_q=v_q^*=0$ in the steady state, (15) is obtained by equating (9) to zero and solving for $\hat{\theta}_i$.

$$\hat{\theta}_i=\theta_i+\frac{3}{3+\gamma+\beta}E_{pu}\cos\left(2\theta_i-\phi_{pu}\right)+\frac{(V_5+V_7)}{V_1}\cdot\cos\left(6\theta_i+\frac{\pi}{2}\right)+ \\ +\frac{(V_{11}+V_{13})}{V_1}\cdot\cos\left(12\theta_i+\frac{\pi}{2}\right)+\ldots \quad (15)$$

From (15) it is concluded that the estimated phase has a certain amount of undesired ripple if the utility grid is not ideal, and the SRF-PLL is not correctly designed (i.e. if the undesired harmonics are not filtered out).

In Fig. 2 it is depicted the Bode plot of the disturbance attenuation transfer function shown in (5), when the SRF-PLL is designed according to the parameters shown in Table I. K_p and K_i are the proportional and the integral gains of the PI regulator, f_s is the sampling frequency of the discretized SRF-PLL, β_V is the sensing gain previous to the ADC stage, *PM* is the phase margin and *GM* is the gain margin. The Bode plot reveals that the harmonics due to the PCC voltage disturbances (i.e. unbalance and harmonic distortion) are poorly rejected. In fact, the harmonic due to the PCC voltage unbalance at $2f_i=100Hz$ is amplified, where f_i is the grid voltage fundamental frequency.

The poor rejection behavior of the proposed SRF-PLL is clearly noticeable from the simulation shown in Fig. 3(b), where the voltage at the PCC has been programmed according to Table II. As expected, the estimated phase, $\hat{\theta}_i$, and the q term of the SRF projection, v_q, contains the harmonics shown by (15) and (9) respectively. However, the estimated phase is synchronized with $v_a(t)$, and the q term of the SRF projection is zero when an ideal utility grid (i.e. the utility grid shown by (1)) is used to feed the input of the phase estimator, as it can be seen in Fig. 3(a).

Although the bandwidth of the system could be reduced to obtain a better harmonic rejection, the settling time of the SRF-PLL would be too slow if a good attenuation has to be obtained (e.g. a $BW=35Hz$ allows an attenuation of only $-4.42dB$).

III. Selective Filtering Technique

In order to selectively remove the harmonics due to the disturbances, a set of n second order notch filters can be used in cascade as shown in Fig. 4, each of those filters removing one of the undesired harmonics which appear in v_q, thus allowing to obtain $\hat{\theta}_i = \theta_i$ from (15).

A widely used digital filter structure is the IIR second order

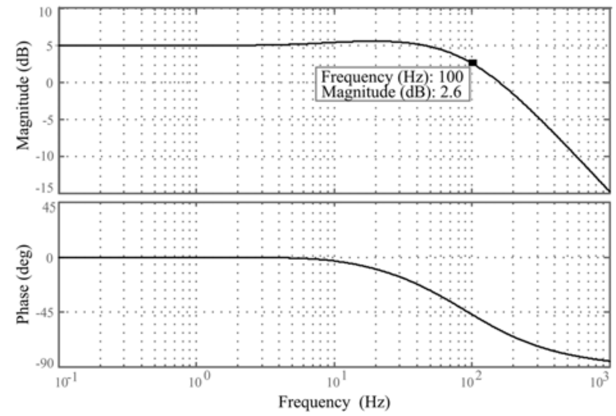

Fig. 2. Attenuation of the disturbances contained in the q term of the SRF-PLL.

TABLE I
PARAMETERS OF THE SRF-PLL AND OF THE IDEAL UTILITY GRID

Parameter	*Value*
V_1	188V
f_i	50Hz
K_p	1114
K_i	63
f_s	16000Hz
β_V	$2.5\cdot 10^{-3}$
PM-f_c	82.3º at 99.7Hz
GM-f	47.1dB at 8000Hz

TABLE II
PARAMETERS OF THE POLLUTED UTILITY GRID

Parameter	*Value*
V_1	188V
$V_5=0.1V_1$	18.8V
$V_7=0.07V_1$	13.2V
$V_{11}=0.05V_1$	8.5V
$V_{13}=0.04V_1$	7.2V
β	-0.1
γ	0.3

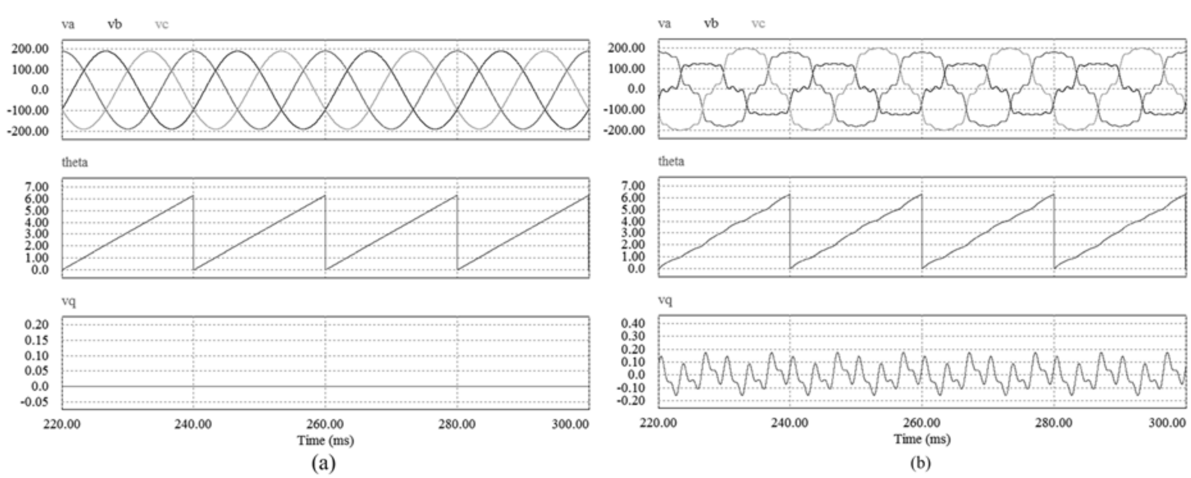

Fig. 3. Three-phase electric grid voltages (top), phase estimation of a SRF-PLL (middle) and v_q signal (bottom) in a (a) non-distorted and non-unbalanced electric grid and (b) distorted and unbalanced electric grid.

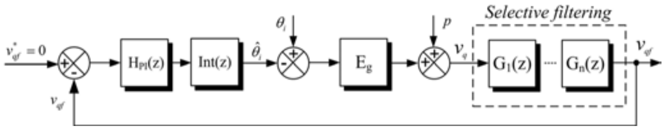

Fig. 4. Small signal block diagram of a SRF-PLL with v_q signal selective filtering.

filter shown by (16), where the tuning parameters a_n and ρ_n are used to set the normalized center frequency, ω_n, and the normalized bandwidth of the notch filter, BW_n, respectively, by using (17) and (18) [35-37]. The z-plane root locus and the Bode plot of the filter for a fixed notching frequency of $\omega_n=2\pi 100 rad/s$ and a sampling frequency of $f_s=16000Hz$, are shown in Fig. 5(a) and in Fig. 5(b), respectively.

The use of the proposed filters modifies both the open loop gain, T_{PLL}, and the disturbance attenuation of the v_q signal, G_{θ_p}, so that (4) turns into (19), and (5) into (20). $G_1(z)\cdot\ldots\cdot G_n(z)$ are the transfer functions product of the n notch filters used to filter out the disturbances. Note that (19) and (20) are discrete versions of (4) and (5) adding the discrete notch filters, where *Int(z)* is a discrete integrator.

$$G_n(z)=\frac{1+a_n z^{-1}+z^{-2}}{1+\rho_n a_n z^{-1}+\rho_n^2 z^{-2}}, \quad -2<a_n<2 \tag{16}$$

$$\omega_n=\cos^{-1}(-a_n/2) \text{ rad} \tag{17}$$

$$BW_n=\pi(1-\rho_n) \text{ rad} \tag{18}$$

$$T_{PLL}^{'}(z)=-E_g\cdot H_{PI}(z)\cdot G_1(z)\cdot\ldots\cdot G_n(z)\cdot Int(z) \tag{19}$$

$$G_{\theta\_p}^{'}(z)=\frac{1}{E_g}\frac{T_{PLL}^{'}(z)}{1+T_{PLL}^{'}(z)} \tag{20}$$

The most important disturbances are those related with the PCC voltage unbalance and the fifth, seventh, eleventh and thirteenth PCC NRF voltage harmonics [33], [34]. Therefore it is possible to use only three notch filters in the SRF, so that the disturbances described in (13) and (14) are removed

It is worth pointing out that the use of the notch filters in the closed loop control of the SRF-PLL introduces new constraints when designing the PI regulator. The phase margin depends on the bandwidth of the notch filter, because the low frequency phase delay of a notch is higher the greater its bandwidth, as it is depicted in Fig. 5(b). Taking this into account, a new SRF-PLL which includes the notch filters can be designed according to the parameters shown in Table III.

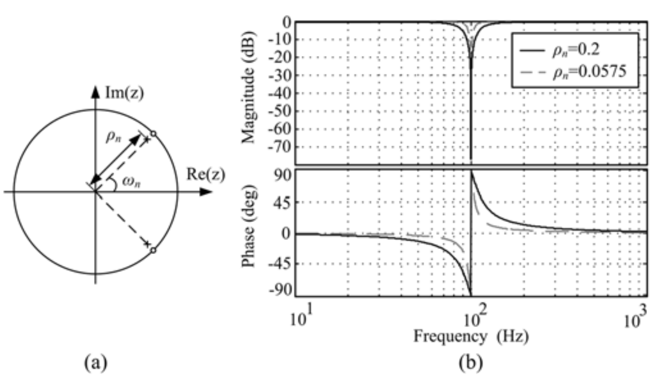

Fig. 5. Digital second order notch filter (a) root locus and (b) Bode plot.

The Bode plot of the disturbance rejection transfer function with notches, $G_{\theta\_p}^{'}(z)$, is shown in Fig. 6. The notch filters allow the SRF-PLL to correctly reject the second, sixth and twelfth harmonics, since they provide an attenuation of nearly -50dB. However, if there is a variation of the PCC voltage frequency, the attenuation will greatly decrease (e.g. a -6% PCC voltage frequency variation will cause the harmonics to be attenuated only by -3.85dB). As it would be desirable to have a constant attenuation regardless of a possible PCC voltage frequency variation, a technique for adaptive filtering of the disturbances is presented below.

IV. Adaptive Filtering

The selective filtering of the harmonics due to the disturbance at the PCC voltage allows the SRF-PLL to obtain a correct estimation of the phase. However, when the frequency of the PCC voltage varies, the highly selective notch filters do not correctly work, because the notch frequencies, ω_n, are fixed.

In order to adapt the notch frequency of the filters according to the PCC voltage fundamental frequency, a finite impulse response (FIR) or infinite impulse response (IIR) adaptive notch filter can be used instead [37], [38].

TABLE III
PARAMETERS OF THE SELECTIVE FILTERING SRF-PLL

Parameter	*Value*
K_p	477.46
K_i	31.42
f_s	16000Hz
β_V	$2.5\cdot 10^{-3}$
$PM\text{-}f_c$	77.2º at 43.2Hz
$GM\text{-}f$	54.5dB at 8060Hz
f_s	16000Hz
ω_1	$2\pi(2\cdot 50)/f_s$ rad
ω_2	$2\pi(6\cdot 50)/f_s$ rad
ω_3	$2\pi(12\cdot 50)/f_s$ rad
$BW_1=BW_2=BW_3$	$2\pi(20)/f_s$ rad

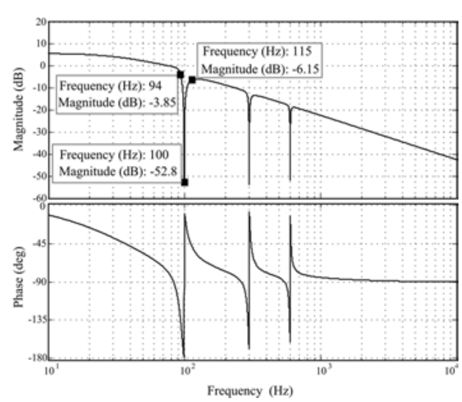

Fig. 6. Attenuation of the disturbances contained in the v_q signal when using the selective filters.

The adaptive filters are based on the use of a recursive algorithm to find the Wiener solution of an error surface that could be time variant (e.g. a surface dependent on the varying frequency of the PCC voltage). Although there are several methods that could be used to implement the recursive algorithm, the most widely used is the *Least Mean Squares* (LMS) algorithm [39-43]. This method is intended to find the parameters of the function $\hat{H}(z)$ defined in (21) that minimizes the quadratic error of the function defined in (22), where $H(z)$ is the transfer function of a given plant and $\zeta(z)$ is a disturbance signal statistically independent of the input signal, $u(z)$.

$$\hat{H}(z)=\frac{B(z)}{A(z)}=\frac{b_0+b_1z^{-1}+\cdots+b_M z^{-M}}{1+a_1z^{-1}+\cdots+a_M z^{-M}} \quad (21)$$

$$e(z)=y(z)-\hat{y}(z)=\left[H(z)-\hat{H}(z)\right]u(z)+\zeta(z) \quad (22)$$

Although this method provides a good performance when applied to a FIR filter, an unstable filter could be obtained if it is used along with a direct form type IIR filter, since the poles of the discrete transfer function are not constrained to lay inside the unity circle [35], [36]. Although a FIR filter could be used to obtain an adaptive notch filter, the computational burden and the need of a given reference signal for the filter to work properly, makes this topology less attractive than the equivalent adaptive notch IIR filter. As it will be shown later, the IIR filter does not need a reference signal to cancel out the undesired harmonics. Furthermore, a second order IIR filter suffices to achieve this goal, while a higher order FIR filter is necessary to obtain the same filtering behavior, thus incrementing the computational burden [44]. In order to find a stable adaptive notch IIR filter, the lattice structure and the gradient adaptive lattice algorithm is presented next.

A. The Schur-Lattice IIR structure

The Schur-lattice IIR structure is based on the Schur recursion depicted in Fig. 7(a), which carries out the rotation over the transfer functions involving the filtering process expressed in (23), where (24) applies.

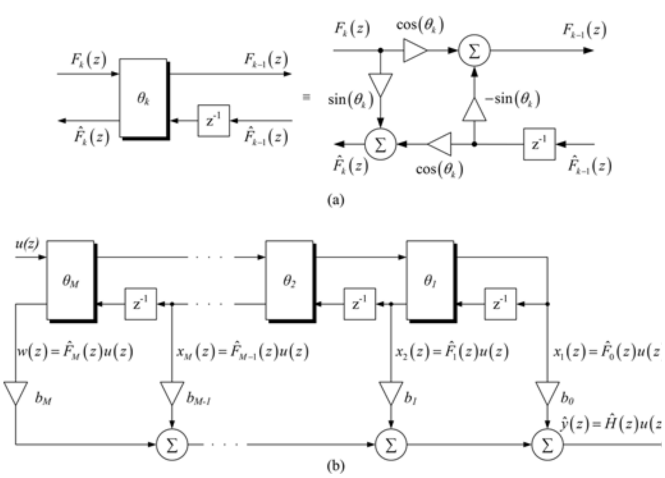

Fig. 7. (a) Schur recursion and (b) *M*th order Schur-Lattice IIR filter.

$$\begin{bmatrix} F_{k-1}(z) \\ \hat{F}_k(z) \end{bmatrix}=\begin{bmatrix} \cos(\theta_k) & -\sin(\theta_k) \\ \sin(\theta_k) & \cos(\theta_k) \end{bmatrix}\begin{bmatrix} F_k(z) \\ z^{-1}\hat{F}_{k-1}(z) \end{bmatrix} \quad (23)$$

$$F_k(z)\triangleq D_k(z)\big/D_M(z), \qquad \hat{F}_k(z)\triangleq \hat{D}_k(z)\big/D_M(z) \quad (24)$$

$$\hat{H}(z)=\sum_{k=0}^{M} b_k\hat{F}_k(z) \quad (25)$$

Fig. 7(b) depicts an *Mth* order IIR filter implemented by means of the Schur recursion, whose transfer function can be expressed by (25). This structure is also known as the tapped state lattice form, and it has many desirable properties for fixed coefficient digital filtering [32]:

- The structure is inherently limited to realizing stable and causal filters. This means that the adaptation process cannot result in an unstable filter.
- All the internal nodes are inherently scaled in the l_2 sense (also known as the Euclidean norm). This property assures that the same Q-format could be used to program the filter, so that precision is not lost in the filtering process.
- Round-off noise accumulation in the state vector loop is inherently low irrespective of the poles of the filter. In this regard, the mapping of the poles and zeros is more precise no matter the position of the poles and zeros. This property is very interesting in low-frequency signal high-frequency sampling.
- Quantization limit cycles due to quantization can be easily suppressed.

It should be noted that these properties allow obtaining a more effective filtering with less ripple due to the adaptive process than in previously proposed adaptive methods.

B. Stability of the Schur-Lattice IIR structure

It is well known that the proposed Schur-lattice IIR structure is inherently stable [32], [45], [46]. Indeed, this property could be probed by using the Schur-Cohn stability test [47], which states that a function $f_0(z)$ is bounded real *iff* (if and only if) (i) $\left|f_0(0)\right|<1$ and (ii) the function $f_1(z)$ defined by (26) is bounded real. The function $f_1(z)$ could be tested in the same way, thus obtaining the sequence of functions $f_0(z), f_1(z),\ldots, f_M(z)=1$. By calculating the sequence of numbers $f_0(0), f_1(0),\ldots, f_{M-1}(0)$ (i.e. the Schur parameters), the Schur-Cohn stability test establishes that $f_0(z)$ is bounded real *iff* all the Schur parameters are smaller than one.

$$f_1(z)=z^{-1}\frac{f_0(z)-f_0(0)}{1-f_0(z)f_0(0)} \quad (26)$$

This test could be applied to the transfer functions $f_0(z)=\hat{F}_M(z)=\hat{D}_M(z)\big/D_M(z)$ to prove the stability of the proposed filter. As $f_0(z)$ is an all-pass function, whose denominator and numerator are expressed by $D_M(z) = A(z)$ and $\hat{D}_M(z) = z^{-M} D_M(z^{-1})$ respectively, it can be affirmed that $\hat{H}(z)$ is stable *iff* $\hat{F}_M(z)$ is stable [47].

On one hand, by using (26) in (23), an expression for $\hat{D}_{k-1}(z)$ as well as for $D_{k-1}(z)$ can be obtained. On the other hand, by studying both transfer functions for *k=M*, (27) yields, which shows up that $\sin(\theta_M) = f_0(0)$ is the first Schur parameter. Furthermore, a straightforward recursive operation over (27) gives (28), so that according to the Schur-Cohn stability test, the IIR transfer function shown in (25), $\hat{H}(z)$, will be stable *iff* (29) holds.

$$f_1(z) = \frac{\hat{D}_{M-1}(z)}{D_{M-1}(z)} = z^{-1} \frac{\hat{D}_M(z)\big/D_M(z) - \sin(\theta_M)}{1 - \hat{D}_M(z)\big/D_M(z)\,\sin(\theta_M)} \quad (27)$$

$$f_k(0) = \frac{\hat{D}_{M-k}(0)}{D_{M-k}(0)} = \sin(\theta_{M-k}), \quad k = 0,\ 1,\ \ldots,\ M-1 \quad (28)$$

$$\left|\sin(\theta_{M-k})\right| < 1 \quad (29)$$

It is important pointing out that (29) is always true except for the angles $\theta_{M-k} = \pm\pi/2$. However, if this condition arises then the all-pass function becomes $f_k(z) \equiv 1$, as the zeros and the poles are located at the unit circle and consequently they cancel out. Moreover, the Schur recursion makes these reciprocal roots to cancel out at the output of the filter because of the same reason [32].

It should be noted that the obtained conclusion about stability is of a great interest when put together with the LMS algorithm. Since the recursive algorithm is designed to find the Wiener solution by adapting the filter coefficients of the filter, the use of the Schur-Lattice IIR structure proposed in Fig. 7(b), gives an inherently stable IIR filter regardless of the filter coefficients adaptation process.

C. The Gradient Adaptive Lattice Algorithm (GAL)

The aforementioned LMS method can be applied to the Schur-lattice IIR structure, so that the coefficients of the filter are recursively adapted in order to minimize the quadratic error function shown in (22). The recursive algorithm shown in (30) is obtained, where $e(n) = y(n) - \hat{y}(n)$ is the error signal, μ is the learning rate of the adaptive filter, and the filtered regressors could be obtained by applying (31).

$$\begin{bmatrix} b_0(n+1) \\ \vdots \\ b_M(n+1) \\ \theta_1(n+1) \\ \vdots \\ \theta_M(n+1) \end{bmatrix} = \begin{bmatrix} b_0(n) \\ \vdots \\ b_M(n) \\ \theta_1(n) \\ \vdots \\ \theta_M(n+1) \end{bmatrix} + \mu e(n) \begin{bmatrix} \nabla b_0(n) \\ \vdots \\ \nabla b_M(n) \\ \nabla\theta_1(n) \\ \vdots \\ \nabla\theta_M(n) \end{bmatrix} \quad (30)$$

$$\begin{aligned} &\nabla b_k(z) = x_{k+1}(z), \quad k = 0,\ 1,\ \ldots,\ M-1 \\ &\nabla b_M(z) = w(z), \quad k = M \\ &\nabla\theta_k(z) = \frac{\partial y(z)}{\partial\theta_k}, \quad k = 0,\ 1,\ \ldots,\ M \end{aligned} \quad (31)$$

D. Adaptive Schur-Lattice IIR notch filter

A Schur-lattice IIR notch filter is depicted in Fig. 8, which it is based on the Schur-lattice IIR filter realization depicted in Fig. 7. This filter realization performs the transfer function shown in (32), where *AP(z)* is the all-pass transfer function defined in (33). The filter allows the designer to adjust the notch frequency as well as the bandwidth by means of (34) and (35) respectively. The angles of the rotation matrix will be used to properly tune the notch filter.

$$\hat{G}_n(z) = \frac{1}{2}\left[1 + AP(z)\right] \quad (32)$$

$$AP(z) = \frac{\sin(\theta_2) + \sin(\theta_1)\left(1 + \sin(\theta_2)\right)z^{-1} + z^{-2}}{1 + \sin(\theta_1)\left(1 + \sin(\theta_2)\right)z^{-1} + \sin(\theta_2)z^{-2}} \quad (33)$$

$$\omega_0 = \theta_1 + \frac{\pi}{2}, \qquad |\theta_1| < \frac{\pi}{2} \quad (34)$$

$$\sin(\theta_2) = \frac{1 - \tan\left(BW\big/2\right)}{1 + \tan\left(BW\big/2\right)} \quad (35)$$

As shown in Fig. 6, the main problem of the fixed notches filters is its inability to adjust the center frequency if the utility grid frequency varies. The adaptive Schur-lattice IIR notch filter can be used to overcome this drawback, by using the GAL algorithm to automatically adapt the θ_1 parameter.

In order to find a solution to the GAL algorithm for the Schur-lattice IIR notch filter, the input signal of the filter, *u(n)*, is defined according to (36), where $\{\zeta(\cdot)\}$ is an error signal statistically independent of *u(n)*, p_1 is the amplitude of a sinusoidal signal of frequency ω_1 and T_m is the sampling period of the discrete system.

$$u(n) = p_1 \sin(\omega_1 T_m n) + \zeta(n) \quad (36)$$

By defining the frequency response of the ideal notch filter as shown in (37), and taking into account that the output of the filter could be written as $y(z) = \hat{G}_n(z)\left[u(z) + \zeta(z)\right]$, the variance of the filter output is obtained by means of (38), where σ_ζ^2 is the variance of the input noise, and $\left\|\hat{G}_n(z)\right\|_2$ is the L_2 norm of $\hat{G}_n(z)$.

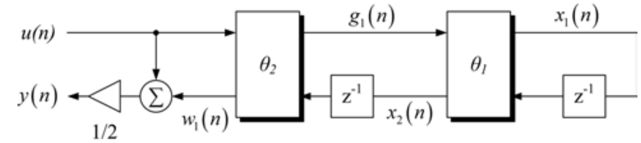

Fig. 8. A second order Schur-lattice IIR notch filter.

$$\left|\hat{G}_n\left(e^{j\omega}\right)\right| = \begin{cases} 0, & \omega = \{\omega_0, -\omega_0\} \\ 1, & \omega \neq \{\omega_0, -\omega_0\} \end{cases} \quad (37)$$

$$E\left[y^2(n)\right] = p_1^2 \left|\hat{G}_n\left(e^{j\omega_1}\right)\right|^2 + \sigma_\zeta^2 \left\|\hat{G}_n(z)\right\|_2^2 \quad (38)$$

By substituting (37) in (38), and assuming that the center frequency of the Schur-lattice IIR notch filter can vary according to the GAL algorithm that will be proposed shortly, (39) yields, from which it is possible to affirm that the function $E\left[y^2(n)\right]$ has a minimum when the condition $\omega_0 = \omega_1$ is satisfied.

$$E\left[y^2(n)\right] = \begin{cases} \sigma_\zeta^2 \left\|\hat{G}_n(z)\right\|_2^2, & \omega_0 = \omega_1 \\ p_1^2 + \sigma_\zeta^2 \left\|\hat{G}_n(z)\right\|_2^2, & \omega_0 \neq \omega_1 \end{cases} \quad (39)$$

It can be proved that $\left\|\hat{G}_n(z)\right\|_2^2 = 0.5\left(1+\sin(\theta_2)\right)$, so that it does not vary with the parameter θ_1. Therefore, and considering (39), the cost function chosen to be minimized by the GAL algorithm is shown by (40).

$$J = \frac{\partial E\left[y^2(n)\right]}{\partial \theta_1} \quad (40)$$

Moreover, by carefully examining (38), it could be affirmed that minimizing $E\left[y^2(n)\right]$ respect to θ_1 is equivalent to find the solution for $\left|\hat{G}_n\left(e^{j\omega_1}\right)\right| = 0$. Taking into account the ideal frequency response of the notch filter, this is equivalent to make $\omega_0 = \omega_1$, thus yielding $\theta_1 = \omega_1 + \frac{\pi}{2}$. This solution implies that the GAL Schur-lattice IIR filter does not need a reference to adaptively tune its center frequency. Hence, it is not necessary to feedback the estimated frequency.

In order to apply the GAL algorithm to the Schur-lattice IIR notch filter depicted in Fig. 8, the filtered regresor $\nabla\theta_1(z)$ has to be computed. By using (32), (41) holds, where $T = 0.5\left(\cos(\theta_1)\cos^2(\theta_2)\right)$, $c_1 = \sin(\theta_1)\left(1+\sin(\theta_2)\right)$ and $c_2 = 1+\sin(\theta_2)$.

$$\nabla\theta_1(z) = \frac{\partial y(z)}{\partial \theta_1} = Tz^{-1} \frac{1-z^{-2}}{\left(1+c_1 z^{-1} + c_2 z^{-2}\right)^2} u(z) \quad (41)$$

The schematic of the adaptive Schur-lattice IIR notch filter is depicted in Fig. 9, which could be implemented by means of the simplified GAL algorithm shown in Table IV [32]. A pseudo-code can be found in an Appendix at the end of this paper which clearly states the correct programing sequence.

E. The Adaptive Lattice SRF-PLL

The Adaptive Lattice SRF-PLL (ALSRF-PLL) is just a modified phase estimator derived from that depicted in Fig. 4,

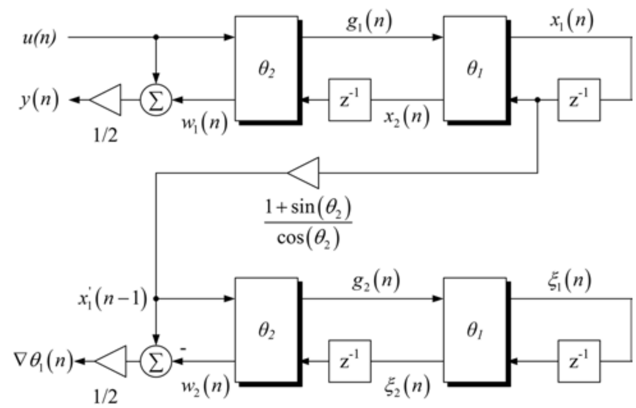

Fig. 9. A second order GAL Schur-lattice IIR notch filter.

TABLE IV
SIMPLIFIED GAL ALGORITHM APPLIED TO THE SCHUR-LATTICE IIR NOTCH FILTER

Filter Parameters Computing
$\begin{bmatrix} g_1(n) \\ w_1(n) \end{bmatrix} = \begin{bmatrix} \cos(\theta_2) & -\sin(\theta_2) \\ \sin(\theta_2) & \cos(\theta_2) \end{bmatrix} \begin{bmatrix} u(n) \\ x_2(n-1) \end{bmatrix}$
$\begin{bmatrix} x_1(n) \\ x_2(n) \end{bmatrix} = \begin{bmatrix} \cos(\theta_1(n)) & -\sin(\theta_1(n)) \\ \sin(\theta_1(n)) & \cos(\theta_1(n)) \end{bmatrix} \begin{bmatrix} g_1(n) \\ x_1(n-1) \end{bmatrix}$
$y(n) = \frac{1}{2}\left[u(n) + w_1(n)\right]$
Filter Parameters Adaptation
$\theta_1(n+1) = \theta_1(n) - \mu y(n) x_1(n-1)$

where the fixed notch filters, $G_1(z)$, …, $G_n(z)$ have been replaced by the GAL Schur-lattice IIR notch filter depicted in Fig. 9, called $\hat{G}_2(z)$, $\hat{G}_6(z)$ $\hat{G}_{12}(z)$. Fig. 10(a) shows the simplified block diagram of the ALSRF-PLL, which includes the adaptive filtering stage. The small signal model is depicted in Fig. 10(b). Each of the used adaptive filters adapts its notch frequency to each of the disturbances considered. As previously stated, this adaptation does not need any reference signal, as the GAL algorithm automatically finds out each of the undesired harmonics. It is worth pointing out that, since the filters are cascade connection, once a harmonic has been removed by the previous stage, next stage will not find it again. In this regard, the transitory ripple in the estimated frequency does not affect the adaptation process, since it is no needed at all.

In order to initialize the ALSRF-PLL, the values of the parameters shown in Table V are used. $\theta_1\_h(initial)$ is the initial value of the parameter θ_1 of the filter designed to reject the h^{th} harmonic (i.e. 2^{nd}, 6^{th} or 12^{th}). μ_h is the learning rate of the adaptive notch filter with initial notch frequency equal to the h^{th} harmonic. Finally, θ_2 is related with the bandwidth of the filter according to (35). It is worth pointing out that a low Q filter is usually designed when using fixed frequency notches, because this assure a better filtering performance even if the frequency varies. As the adaptive filter

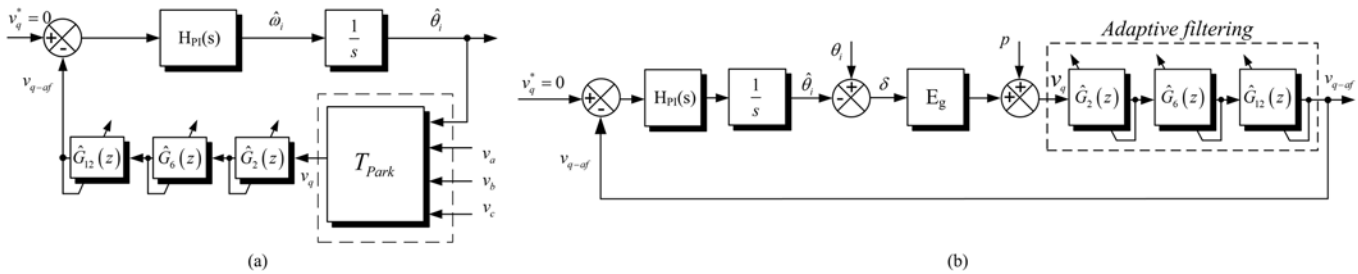

Fig. 10. (a) Basic block diagram and (b) small signal block diagram of an ALSRF-PLL.

TABLE V
PARAMETERS OF THE ALSRF-PLL

Parameter	*Value*
θ_1_2 (initial)	-1.531526418
ω_0_2	2π100 rad/s
θ_2_2	1.445132620
BW_2	20 Hz
μ_2	0.0001
θ_1_6 (initial)	-1.452986602
ω_0_6	2π300 rad/s
θ_2_6	1.445132620
BW_6	20 Hz
μ_6	0.0001
θ_1_12 (initial)	-1.335176877
ω_0_12	2π600 rad/s
θ_2_12	1.445132620
BW_12	20 Hz
μ_12	0.01

automatically adapts its center frequency, a low Q is not required. In this regard, a trade-off between speed convergence during transitory times and phase margin of the ALSRF-PLL has to be found. Usually, θ_2 is chosen so that enough phase margin is obtained at the crossover frequency, when the frequency of the voltage grid is on the minimum considered, while maintaining the equivalent SRF-PLL speed of convergence when a variation on the frequency appears.

V. EXPERIMENTAL RESULTS

The ALSRF-PLL has been implemented into the fixed point DSP TI TMS320F2812. The three-phase utility grid voltage has been emulated by means of the 12kVA AC power source Pacific Power 360-AMX. The AC power source has been programmed so that an unbalance and distorted grid suddenly appears. At a given moment, the frequency of the unbalanced and distorted voltage grid described in (7) and Table II abruptly varies. Therefore, an inherit phase-angle jump is also taken into account. The open loop gain of the ALSRF-PLL, $\hat{T}_{PLL}(z) = -E_g H_{PI}(z)\hat{G}_2(z)\hat{G}_6\hat{G}_{12}(z)Int(z)$, has been measured by means of the frequency response analyzer (FRA) NF FRA5097 [48]. The real time data has been read from the DSP by using the RTDX core [49]; MATLAB has been used to process and to plot the collected data. The obtained Bode plots are depicted in Fig. 11, for the nominal, the minimum and the maximum frequencies under study, i.e. 50Hz, 45Hz, and 55Hz, respectively. The chosen frequencies are according to the nominal, minimum and maximum frequency included in norms as the UNE-EN 50160 [50].

On the one hand, the correct behavior of the adaptive filters is clearly appreciable in Fig. 11, as the notch frequency of each of the filters varies according to the frequency variation of the grid voltage. On the other hand, it should be noted that the minimum phase margin is *PM=73.5º* at f_c*=44Hz*, when the frequency of the grid voltage at the PCC is f_i*=45Hz*, whereas the maximum phase margin is *PM=77.2º* at f_c*=44Hz* when f_i*=55Hz*. The nominal phase margin is *PM=75.3º* at f_c*=44Hz* when f_i*=50Hz*. Those phase margins are high enough to assure that the ALSRF-PLL is stable when the grid voltage frequency at the PCC varies from f_i*=45Hz* to f_i*=55Hz*.

In Fig. 12 it is depicted the unbalance and distorted three-phase utility grid voltages used to test the conventional SRF-PLL, the fixed notch filtered SRF-PLL and the ALSRF-PLL. First of all, the conventional SRF-PLL has been programmed into the DSP, so that the estimated phase can be obtained

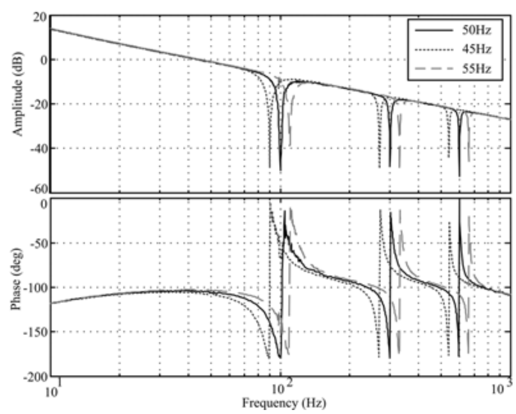

Fig. 11. Experimental open loop gains, T'_{PLL}, of the ALSRF-PLL for the maximum, the minimum, and the nominal considered electric grid frequencies.

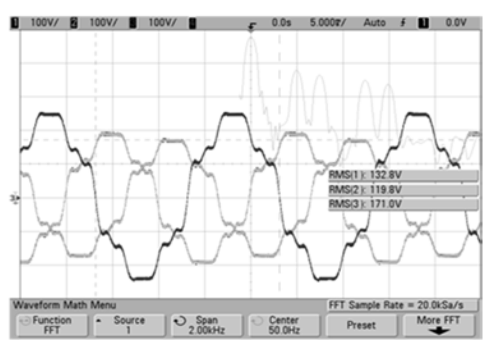

Fig. 12. Unbalanced and distorted three-phase utility grid AC power source voltages.

when the utility grid voltage is heavily distorted and unbalance. Fig. 13(a) shows the sensed $v_{ab}(t)$ voltage (i.e. the phase to phase voltage), where the harmonic distortion is clearly appreciable. In Fig. 13(b) it is shown the estimated phase, $\hat{\theta}_i$, where it is possible to notice that a ripple exists due to the 2nd, the 6th and the 12th harmonics. Furthermore, in the $v_q(t)$ signal depicted in Fig. 13(c), the ripple is much more appreciable. A sinusoidal signal, $\sin(\hat{\theta}_i)$, has been generated by means of the estimated phase shown in Fig. 13(b), and the FFT of this signal has been computed, thus obtaining the result shown in Fig. 14. This result clearly shows the 1st harmonic (i.e. 50Hz), the 3rd harmonic (i.e. 150Hz), the 5th harmonic (i.e. 250Hz), the 7th harmonic (i.e. 350Hz), the 11th harmonic (i.e. 550Hz) and the 13th harmonic (i.e. 650Hz). It should be noted that the 3rd harmonic is due to the effect of the reference frame translation to the unbalance harmonic in the SRF, so that this harmonic (i.e 2nd harmonic), behaves like the 3rd harmonic in the NRF.

In order to remove these unwanted harmonics, which degrade the current THD of the converter current [9], the fixed notch filters previously described have been included. The filtered SRF-PLL behavior has been tested both at the nominal grid frequency and at a grid frequency different from the nominal one. In order to set up the experiment, the AC power source has been programmed so that the initial condition of the emulated grid voltage has neither unbalance nor harmonic distortion. At a given instant of time, the grid voltage is varied so that it contains the aforementioned unbalance and harmonic distortion, whereas maintaining the same frequency (i.e. the nominal frequency of 50Hz). Finally, the frequency of the distorted and unbalance three-phase grid voltage is varied from the nominal one (i.e. 50Hz), to the maximum frequency considered (i.e. 55Hz.), and then the three-phase grid voltage is returned to the initial condition (i.e. neither unbalance nor distortion with a frequency of 50Hz).

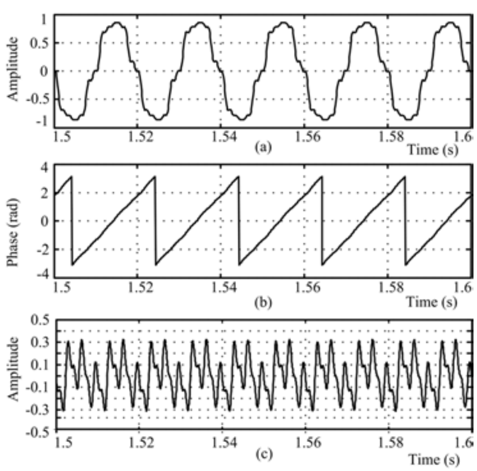

Fig. 13. Experimental (a) sensed line voltage, V_{ab}, (b) estimated phase, $\hat{\theta}_i$ and (c) v_q signal for the unbalanced and distorted electric grid shown in Fig. 12.

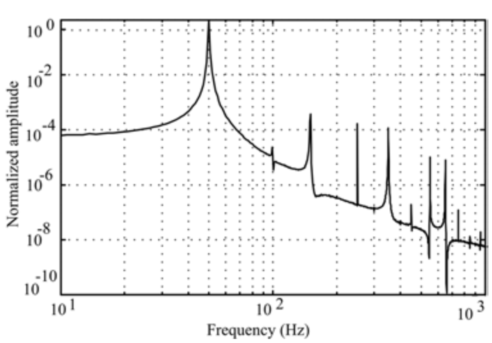

Fig. 14. FFT of a sinusoidal reference, $\sin(\hat{\theta}_i)$, obtained by means of the estimated phase, $\hat{\theta}_i$, of a conventional SRF-PLL.

Fig. 15 shows the $v_q(t)$ and the filtered $v_{qf}(t)$ signals of the notch filtered SRF-PLL when: 1. (from t≈0s until t≈0.5s) Neither unbalance nor distortion exists, and the frequency is 50Hz; 2. (from t≈0.5s until t≈1.5s) The unbalance and the distortion are abruptly introduced, maintaining the nominal frequency 3. (from t≈1.5 until t≈2.5s) The frequency of the distorted and unbalanced set of voltages is varied from 50Hz to 55Hz. It is worth mentioning that the t=0s has been chosen to be the moment the RTDX algorithm starts sending data to the PC, and not the moment the notch filtered SRF-PLL starts working. In fact, the notch filtered SRF-PLL is in its steady state when the change of the voltage frequency takes place, so that the start-up sequence of the synchronization algorithm is not shown. Anyway, as the initial conditions of the SRF-PLL is chosen to be $\hat{\omega}_i = 2\pi \hat{f}_i$ rad/s, where $\hat{f}_i$ is the expected grid frequency, the start-up transient is not important compared to the transient due to the variation of the voltage grid frequency.

As the notch filters are designed by considering a fixed nominal frequency of 50Hz, they perform as expected from t≈0s until t≈0.5s, since the ripple in $v_{qf}(t)$ is strongly filtered out. However, when the nominal frequency varies from 50Hz to 55Hz, the filters are not able to reject the disturbances, so that the $v_{qf}(t)$ signal does contain almost all the ripple found in the $v_q(t)$ signal. This is conveniently shown in Fig. 16(a) and Fig. 16(b), where the FFT of the normalized $v_q(t)$ and $v_{qf}(t)$ signals (i.e. respect to the 3rd harmonic amplitude), has been computed when the grid frequency is (a) 50Hz, and (b)55Hz.

By examining both plots, it is possible to affirm that the 2nd, 6th and 12th harmonics are strongly attenuated when the

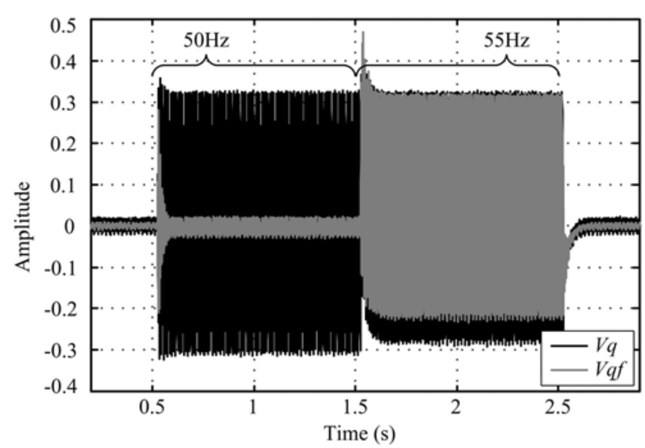

Fig. 15. v_q (black) and v_{qf} (grey) signals of a selective filtered SRF-PLL, for the unbalanced and distorted electric grid shown in Fig. 12, when the frequency is tuned at 50Hz and at 55Hz.

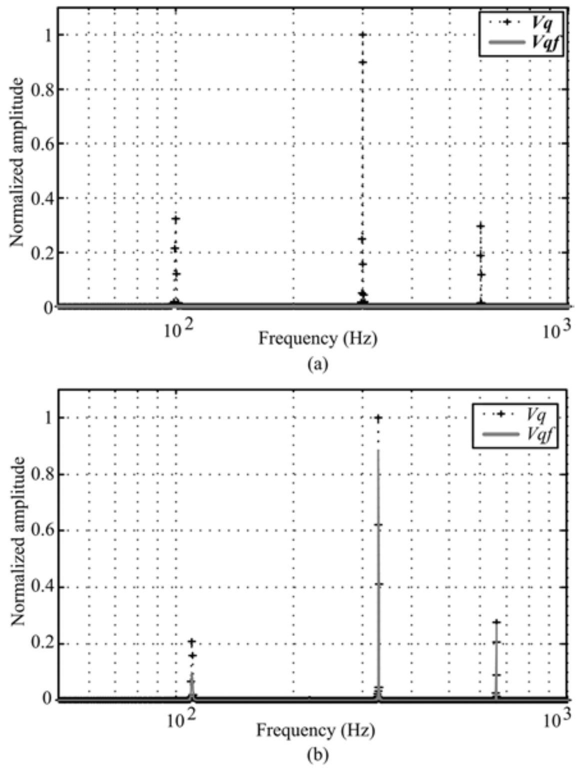

Fig. 16. Normalized v_q (black-dotted) and v_{qf} (grey-solid) signals of a selective filtered SRF-PLL, for the unbalanced and distorted electric grid shown in Fig. 12 when the frequency is tuned at (a) 50Hz and (b) 55Hz.

frequency is fixed and equal to the nominal one (i.e. 50Hz). However, those harmonics are still at the output of the fixed notches when the frequency of the fundamental harmonic varies. This has been numerically evaluated by means of the attenuation value shown in Table VI. As previously stated, the ripple on the $v_{qf}(t)$ signal, (and thus the ripple on the estimated phase), can be found at the sinusoidal reference, $I^* = I_M \sin\left(\hat{\theta}_i\right)$, used to control the current loop of the power converter. Fig. 17 shows the FFT of the $\sin\left(\hat{\theta}_i\right)$ in a non-adaptive selective filtered SRF-PLL, showing that the performance of the power converter is sensitive to a variation on the grid frequency.

The same experiment has been carried out by using the proposed ALSRF-PLL. Fig. 18 shows the $v_q(t)$ and the $v_{q\text{-}af}(t)$ signals when a variation of the aforementioned grid voltage has been programmed in the AC power source. It is worth pointing out that t=0s is chosen to be the moment the RTDX algorithm starts working. Furthermore, the initial coefficients of the adaptive filters have been chosen so that the filters are tuned at the expected harmonic frequency (i.e. second, sixth and twelfth harmonics).

TABLE VI
DISTURBANCES ATTENUATION BY MEANS OF THE IIR FIXED NOTCHES

Harmonic number	Attenuation (dB)	
	50Hz	55Hz
2	-120.2	-6.5
6	-114.1	-1.1
12	-111.2	-0.3

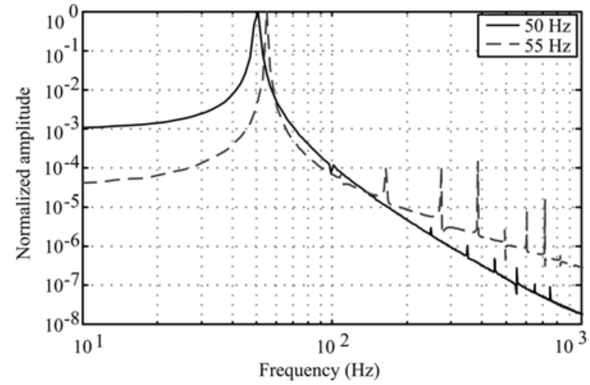

Fig. 17. FFT of a sinusoidal reference, $\sin\left(\hat{\theta}_i\right)$, obtained by means of the estimated phase, $\hat{\theta}_i$, of a selective filtered SRF-PLL, for an unbalanced and distorted electric grid which frequency is 50Hz (black-solid) and 55Hz (grey-dotted).

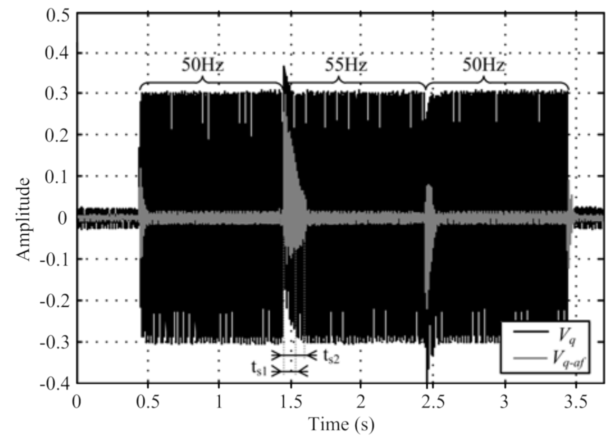

Fig. 18. v_q (black) and $v_{q\text{-}af}$ (grey) of a ALSRF-PLL, for the unbalanced and distorted electric grid shown in Fig. 12, when the frequency is tuned at 50Hz and at 55Hz.

The good performance of the adaptive notch filter implemented by means of the Schur-lattice structure is clearly noticiable, for a ripple-free filtered signal $v_{q\text{-}af}(t)$ is obtained regardless of the frequency of the utility grid. The FFT has been applied to both signals, $v_q(t)$ and $v_{q\text{-}af}(t)$, when the grid frequency is 50Hz and 55Hz. The result is shown in Fig. 19(a) and in Fig. 19(b), respectively. It can be observed that the adaptive notch filter strongly rejects the disturbances in both cases, as shown in Table VII. A sinusoidal reference has been generated by means of the 50Hz and the 55Hz adaptively filtered estimated phase in the steady state. The FFT of these signals are plotted in Fig. 20, from which it is possible to affirm that the harmonics due to the unbalance and the distortion are negligible

It is important pointing out that the convergence or learning rate parameter, μ, has been chosen in order to achieve a compromise between stability and convergence speed. On one hand, the value of μ has to allow obtaining a stable adaptive filter (i.e. a fast filter, with a great μ, could result in an unstable filter). On the other hand, this parameter has to be adjusted so that the time the ALSRF-PLL takes to achieve convergence is similar to the time the conventional SRF-PLL needs to correctly estimate the phase of the first harmonic (i.e.

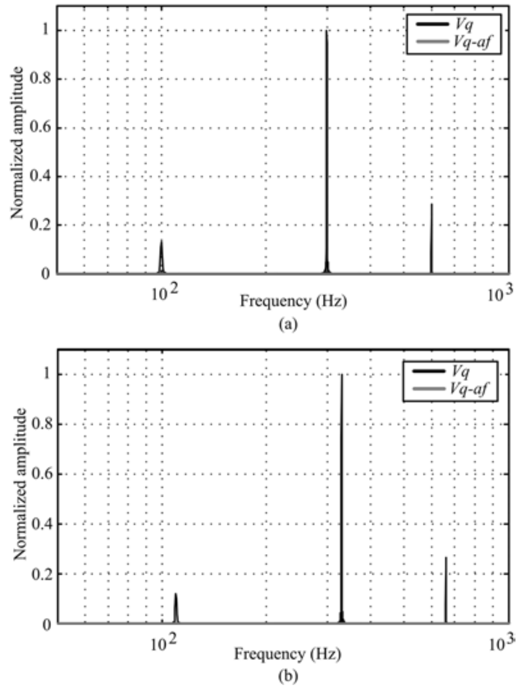

Fig. 19. Normalized v_q (black-solid) and $v_{q\text{-}af}$ (grey-solid) signals of an ALSRF-PLL, for the unbalanced and distorted electric grid shown in Fig. 12 when the frequency is tuned at (a) 50Hz and (b) 55Hz.

TABLE VII
DISTURBANCES ATTENUATION BY MEANS OF THE IIR ADAPTIVE NOTCHES

Harmonic number	*Attenuation (dB)*	
	50Hz	*55Hz*
2	-90.3	-94.5
6	-100.6	-105.0
12	-121.4	-150.7

the greater the μ parameter, the faster the adaptive filter). By achieving these goals, the adaptive IIR filter is stable and it does not make the response of the ALSRF-PLL significantly slower than the conventional SRF-PLL, as can be seen in Fig. 15 and Fig. 18, where $t_{s1}≈0.5s$ is the settling time of the SRF-PLL and $t_{s2}≈0.75s$ is the settling time of the ALSRF-PLL, both measured at 5% of the final value. Although the extra time $t_s≈0.25s$ appears due to the adaptive algorithm, it should be noted that the undesired harmonics of the v_q component are highly attenuated during this transition time. Hence, they do not critically affect the estimated phase during transitions.

The time consumption of each of the studied synchronization methods, along with the attenuation of the 2nd harmonic in the v_q variable, is shown in Table VIII. It should be noted that this attenuation is not applicable to the conventional SRF-PLL, so that it is not shown.

VI. CONCLUSIONS

An SRF-PLL with adaptive disturbance rejection properties has been presented. The ALSRF-PLL is able to strongly reject the disturbances due to the grid voltage unbalance and harmonic distortion regardless of variations of the grid voltage

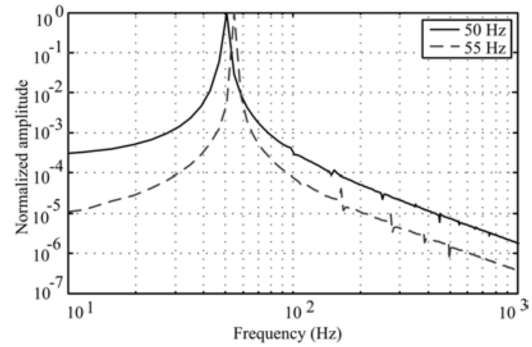

Fig. 20. FFT of a sinusoidal reference, $\sin(\hat{\theta}_i)$, obtained by means of the estimated phase, $\hat{\theta}_i$, of a ALSRF-PLL, for an unbalanced and distorted electric grid which frequency is 50Hz (black-solid) and 55Hz (grey-dotted).

TABLE VIII
TIME CONSUPTION VS. 2ND HARMONIC ATTENUATION

Synchronization method	*Time (µs)*	*2nd harmonic Attenuation (dB)*	
		50Hz	*55Hz*
SRF-PLL	1.7	-	-
SRF-PLL + Fixed Notch	2.7	-120.2	-6.5
ALSRF-PLL	7.9	-90.3	-94.5

frequency. The presented synchronization method is based on the adaptive filtering of the grid voltage q term of the SRF projection. A set of IIR notch filters implemented by the Schur-lattice structure and the GAL recursive method have been used. This structure is inherently stable regardless of the coefficient adaptation process and offers some of the desired properties to be programed into a fixed point DSP. Furthermore, existing SRF-PLL could be easily updated so that they become adaptive. It offers a good chance to add new features to existing power converters, thus improving its original performance.

The experimental results have shown that the stability of the whole ALSRF-PLL system (i.e. SRF-PLL + Schur-lattice + GAL structure) is assured even in the worst case (i.e. when the voltage grid frequency is the minimum one under consideration). Furthermore, the ALSRF-PLL is able to provide large fixed disturbance attenuation, regardless of abrupt variations of the grid voltage frequency and of the grid voltage unbalance. Therefore, the harmonics other than the fundamental of a sinusoidal reference obtained by means of the estimated phase can be considered negligible.

The computational burden of the ALSRF-PLL is quite larger than the SRF-PLL. Although the fixed notch SRF-PLL could be a trade-off solution, it is clearly shown that this synchronization method is not well suited for applications where a variation in the frequency of the voltage grid may occur.

In future works, an improved computational burden is expected to be obtained. Furthermore, the Schur-latice IIR filter could be also exploited so that it becomes the core of the three-phase power converter control scheme.

APPENDIX

In order to clarify the algorithm shown in Table IV, a pseudo code of the filtering process is shown in Fig. 21. The first lines define the constant parameters (i.e. μ_n and θ_2_n, where n is the harmonic number to be filtered out). The global variables are defined next, where the initial values of the θ_1_n variables are chosen so that the IIR adaptive filters are tuned at the expected harmonics frequencies, while the state variables *x1k1_n* could be initialized to zero. The main algorithm code consists of the code for the three filters, where the input of the first one is the v_q component, while its output feds the second one (i.e. they are cascade connected). Eventually, the output of the third filter is the filtered v_q component (i.e. v_{q_af}).

```
//Define constants
constant mu_100 0.0001
...
constant theta2_100 1.445132620
...
//Define global variables
x1k1_100=0;
...
theta1_100=-1.531526418;
...
//Define local variables
w1k_100, g1k_100, x1k_100, x2k_100, yk_100;
...
//Computes the output of the 100Hz notch filter
g1k_100=cos(theta2_100)*vq-sin(theta2_100)*x2k1_100;
w1k_100=sin(theta2_100)*vq+cos(theta2_100)*x2k1_100;
yk_100=0.5*(vq+w1k_100);
//Computes the states of the 100Hz notch filter
x1k_100=cos(theta1_100)*g1k_100-sin(theta1_100)*x1k1_100;
x2k_100=sin(theta1_100)*g1k_100+cos(theta1_100)*x1k1_100;
//Computes the next theta1 parameter of the 100Hz notch filter
theta1_100=theta1_100-mu_100*x1k1_100*yk_100;
//Writes the next states of the 100Hz notch filter
x1k1_100=x1k_100;
x2k1_100=x2k_100;
//Computes the output of the 300Hz notch filter
g1k_300=cos(theta2_300)*yk_100-sin(theta2_300)*x2k1_300;
w1k_300=sin(theta2_300)*yk_100+cos(theta2_300)*x2k1_300;
yk_300=0.5*(yk_100+w1k_300);
…
//Computes the output of the 600Hz notch filter
g1k_600=cos(theta2_600)*yk_300-sin(theta2_600)*x2k1_600;
w1k_600=sin(theta2_600)*yk_300+cos(theta2_300)*x2k1_600;
yk_600=0.5*(yk_300+w1k_600);
…
vq_af=yk_600;
```

Fig. 21. FFT of a sinusoidal reference, $\sin\left(\hat{\theta}_i\right)$, obtained by means of the estimated phase, $\hat{\theta}_i$, of a ALSRF-PLL, for an unbalanced and distorted electric grid which frequency is 50Hz (black-solid) and 55Hz (grey-dotted).

REFERENCES

[1] J. M. Guerrero, F. Blaabjerg, T. Zhelev, K. Hemmes, E. Monmasson, S. Jemei, M. P. Comech, R. Granadino, and J. I. Frau, "Distributed Generation: Toward a New Energy Paradigm," *Industrial Electronics Magazine, IEEE*, vol. 4, no. 1, Mar.2010, pp. 52-64.

[2] H. Rudnick and L. A. Barroso, "On the Winds of Change Impact of Renewables on Electricity Markets [Guest Editorial]," *Power and Energy Magazine, IEEE*, vol. 8, no. 5, Sept.2010, pp. 18-21.

[3] L. Dickerman and J. Harrison, "A New Car, a New Grid," *Power and Energy Magazine, IEEE*, vol. 8, no. 2, Mar.2010, pp. 55-61.

[4] K. J. Dyke, N. Schofield, and M. Barnes, "The Impact of Transport Electrification on Electrical Networks," *Industrial Electronics, IEEE Transactions on*, vol. 57, no. 12, Dec.2010, pp. 3917-3926.

[5] F. Blaabjerg, R. Teodorescu, M. Liserre, and A. V. Timbus, "Overview of Control and Grid Synchronization for Distributed Power Generation Systems," *IEEE Transaction on Industrial Electronics*, vol. 53, no. 5, 2006, pp. 1398-1409.

[6] I. J. Balaguer, L. Qin, Y. Shuitao, U. Supatti, and Z. P. Fang, "Control for Grid-Connected and Intentional Islanding Operations of Distributed Power Generation," *Industrial Electronics, IEEE Transactions on*, vol. 58, no. 1, Jan.2011, pp. 147-157.

[7] O. Carranza, E. Figueres, G. Garcerβ, and L. G. Gonzalez, "Comparative study of speed estimators with highly noisy measurement signals for Wind Energy Generation Systems," *Applied Energy*, vol. 88, no. 3, Mar.2011, pp. 805-813.

[8] E. Figueres, G. Garcera, J. Sandia, F. Gonzalez-Espin, and J. C. Rubio, "Sensitivity Study of the Dynamics of Three-Phase Photovoltaic Inverters With an LCL Grid Filter," *Industrial Electronics, IEEE Transactions on*, vol. 56, no. 3, 2009, pp. 706-717.

[9] M.P.Kazmierkowski, R.Krishnan, and F.Blaabjerg, *Control in Power Electronics. Selected Problems.*, 1st. ed. Academic Press, San Diego, 2002.

[10] S. Hiti, D. Borojevic, R. Ambatipudi, R. Zhang, and J. Yimin, "Average current control of three-phase PWM boost rectifier," *26th Annual Power Electronics Specialists Conference. PESC '95* 1995, pp. 131-137.

[11] C. Lascu, L. Asiminoaei, I. Boldea, and F. Blaabjerg, "Frequency Response Analysis of Current Controllers for Selective Harmonic Compensation in Active Power Filters," *Industrial Electronics, IEEE Transactions on*, vol. 56, no. 2, 2009, pp. 337-347.

[12] D. Velasco, C. Trujillo, G. Garcera, and E. Figueres, "An active Anti-islanding method based on phase-PLL perturbation," *Power Electronics, IEEE Transactions on*, vol. PP, no. 99, 2010, p. 1.

[13] H. Guan-Chyun and J. C. Hung, "Phase-locked loop techniques. A survey," *Industrial Electronics, IEEE Transactions on*, vol. 43, no. 6, 1996, pp. 609-615.

[14] R. M. Santos Filho, P. F. Seixas, P. C. Cortizo, L. A. B. Torres, and A. F. Souza, "Comparison of Three Single-Phase PLL Algorithms for UPS Applications," *Industrial Electronics, IEEE Transactions on*, vol. 55, no. 8, Aug.2008, pp. 2923-2932.

[15] A. Timbus, M. Liserre, R. Teodorescu, P. Rodriguez, and F. Blaabjerg, "Evaluation of Current Controllers for Distributed Power Generation Systems," *Power Electronics, IEEE Transactions on*, vol. 24, no. 3, 2009, pp. 654-664.

[16] C. Se-Kyo, "A phase tracking system for three phase utility interface inverters," *Power Electronics, IEEE Transactions on*, vol. 15, no. 3, 2000, pp. 431-438.

[17] M. Karimi-Ghartemani and M. R. Iravani, "A method for synchronization of power electronic converters in polluted and variable-frequency environments," *Power Systems, IEEE Transactions on*, vol. 19, no. 3, 2004, pp. 1263-1270.

[18] V. Kaura and V. Blasko, "Operation of a phase locked loop system under distorted utility conditions," *Industry Applications, IEEE Transactions on*, vol. 33, no. 1, 1997, pp. 58-63.

[19] "IEEE Recommended Practice for Utility Interface of Photovoltaic (PV) Systems," *IEEE Std 929-2000*, 2000, p. i.

[20] "IEEE Standard for Interconnecting Distributed Resources With Electric Power Systems," *IEEE Std 1547-2003*, 2003, pp. 0-16.

[21] L. N. Amuda, B. J. Cardoso Filho, S. M. Silva, S. R. Silva, and A. S. A. C. Diniz, "Wide bandwidth single and three-phase PLL structures for grid-tied PV systems," *Photovoltaic Specialists Conference, 2000.* B. J. Cardoso Filho, Ed. 2000, pp. 1660-1663.

[22] F. Liccardo, P. Marino, and G. Raimondo, "Robust and Fast Three-Phase PLL Tracking System," *Industrial Electronics, IEEE Transactions on*, vol. 58, no. 1, Jan.2011, pp. 221-231.

[23] F. D. Freijedo, J. Doval-Gandoy, O. Lopez, and E. Acha, "Tuning of Phase-Locked Loops for Power Converters Under Distorted Utility Conditions," *Industry Applications, IEEE Transactions on*, vol. 45, no. 6, Nov.2009, pp. 2039-2047.

[24] S. Hong-Seok, P. Hyun-Gyu, and N. Kwanghee, "An instantaneous phase angle detection algorithm under unbalanced line voltage condition,", 1 ed 1999, pp. 533-537.

[25] J. M. Guerrero, J. C. Vasquez, J. Matas, L. G. de Vicuna, and M. Castilla, "Hierarchical Control of Droop-Controlled AC and DC Microgrids-A General Approach Toward Standardization," *Industrial Electronics, IEEE Transactions on*, vol. 58, no. 1, Jan.2011, pp. 158-172.

[26] J. C. Vasquez, J. M. Guerrero, A. Luna, P. Rodriguez, and R. Teodorescu, "Adaptive Droop Control Applied to Voltage-Source Inverters Operating in Grid-Connected and Islanded Modes," *Industrial Electronics, IEEE Transactions on*, vol. 56, no. 10, Oct.2009, pp. 4088-4096.
[27] S. Lisheng and M. L. Crow, "A novel PLL system based on adaptive resonant filter," 40th North American Power Symposium, 2008. NAPS '08., 2008, pp. 1-8.
[28] A. V. Timbus, M. Ciobotaru, R. Teodorescu, and F. Blaabjerg, "Adaptive resonant controller for grid-connected converters in distributed power generation systems," 21 Applied Power Electronics Conference and Exposition, APEC '06, 2006, p. 6.
[29] F. D. Freijedo, A. G. Yepes, O. pez, A. Vidal, and J. Doval-Gandoy, "Three-Phase PLLs With Fast Postfault Retracking and Steady-State Rejection of Voltage Unbalance and Harmonics by Means of Lead Compensation," *Power Electronics, IEEE Transactions on*, vol. 26, no. 1, Jan.2011, pp. 85-97.
[30] P. Rodriguez, J. Pou, J. Bergas, J. I. Candela, R. P. Burgos, and D. Boroyevich, "Decoupled Double Synchronous Reference Frame PLL for Power Converters Control," *Power Electronics, IEEE Transactions on*, vol. 22, no. 2, 2007, pp. 584-592.
[31] P. Rodriguez, A. Luna, I. Candela, R. Mujal, R. Teodorescu, and F. Blaabjerg, "Multi-Resonant Frequency-Locked Loop for Grid Synchronization of Power Converters Under Distorted Grid Conditions," *Industrial Electronics, IEEE Transactions on*, vol. 58, no. 1, 2011, pp. 127-138.
[32] P. A. Regalia, *Adaptive IIR filtering in signal processing and control*. Marcel Dekker, INC., 1995.
[33] N. Mohan, T. M. Undeland, and W. P. Robbins, *Power Electronics. Converters, applications, and design.*, 3rd. ed. John Wiley & Sons, Inc., 2003.
[34] M. H. Rashid, *Power Electronics Handbook*. Academic Press, 2007, pp. 1-1152.
[35] A. Nehorai, "A minimal parameter adaptive notch filter with constrained poles and zeros," *Acoustics, Speech and Signal Processing, IEEE Transactions on*, vol. 33, no. 4, 1985, pp. 983-996.
[36] P. Stoica and A. Nehorai, "Performance analysis of an adaptive notch filter with constrained poles and zeros," *Acoustics, Speech and Signal Processing, IEEE Transactions on*, vol. 36, no. 6, 1988, pp. 911-919.
[37] S. Haykin, *Adaptive filter theory*. Prentice Hall, 2002.
[38] John G.Proakis and Dimitri G.Manolakis, *Digital Signal Processing. Principles, Algorithms, and Applications.*, 4th ed. Pearson Prentice Hall, 2007.
[39] A. K. Kohli and D. K. Mehra, "Tracking of time-varying channels using two-step LMS-type adaptive algorithm," *Signal Processing, IEEE Transactions on*, vol. 54, no. 7, July2006, pp. 2606-2615.
[40] I. D. Schizas, G. Mateos, and G. B. Giannakis, "Distributed LMS for Consensus-Based In-Network Adaptive Processing," *Signal Processing, IEEE Transactions on*, vol. 57, no. 6, June2009, pp. 2365-2382.
[41] H. Byung-Moon, B. Byong-Yeul, and S. J. Ovaska, "Reference signal generator for active power filters using improved adaptive predictive filter," *Industrial Electronics, IEEE Transactions on*, vol. 52, no. 2, 2005, pp. 576-584.
[42] B. Singh and J. Solanki, "An Implementation of an Adaptive Control Algorithm for a Three-Phase Shunt Active Filter," *Industrial Electronics, IEEE Transactions on*, vol. 56, no. 8, Aug.2009, pp. 2811-2820.
[43] J. Arenas-Garcia, V. Gomez-Verdejo, and A. R. Figueiras-Vidal, "New algorithms for improved adaptive convex combination of LMS transversal filters," *Instrumentation and Measurement, IEEE Transactions on*, vol. 54, no. 6, Dec.2005, pp. 2239-2249.
[44] J. Glover, Jr., "Adaptive noise canceling applied to sinusoidal interferences," *Acoustics, Speech and Signal Processing, IEEE Transactions on*, vol. 25, no. 6, 1977, pp. 484-491.
[45] P. A. Regalia, "Stable and efficient lattice algorithms for adaptive IIR filtering," *Signal Processing, IEEE Transactions on*, vol. 40, no. 2, 1992, pp. 375-388.
[46] A. Gray, Jr. and J. Markel, "A normalized digital filter structure," *Acoustics, Speech and Signal Processing, IEEE Transactions on*, vol. 23, no. 3, June1975, pp. 268-277.
[47] P. P. Vaidyanathan and S. K. Mitra, "A unified structural interpretation of some well-known stability-test procedures for linear systems," *Proceedings of the IEEE*, vol. 75, no. 4, Apr.1987, pp. 478-497.
[48] F. Gonzalez-Espin, E. Figueres, G. Garcera, R. Gonzalez-Medina, and M. Pascual, "Measurement of the Loop Gain Frequency Response of Digitally Controlled Power Converters," *Industrial Electronics, IEEE Transactions on*, vol. 57, no. 8, Aug.2010, pp. 2785-2796.
[49] Texas Instruments, "RTDX 2.0 Reference Guide," 2010.
[50] "Características de la tensión suministrada por las redes generales de distribución," *UNE-EN 50160*, 2011.

Fran González-Espín

.

Emilio Figueres

Gabriel Garcerá